Inorg. Chem. **2007**, *46*, 213–220

Characterization of the Crystal and Magnetic Structures of the Mixed-Anion Coordination Polymer $Cu(HCO_2)(NO_3)(pyz)$ {pyz = Pyrazine} by X-ray Diffraction, ac Magnetic Susceptibility, dc Magnetization, Muon-Spin Relaxation, and Spin Dimer Analysis

J. L. Manson,*,†,‡ T. Lancaster,§ J. A. Schlueter,£ S. J. Blundell,§ M. L. Brooks,§ F. L. Pratt,|| C. L. Nygren,⊥ H.-J. Koo,# D. Dai,▽ and M.-H. Whangbo▽

Condensed Matter Sciences Division, Oak Ridge National Laboratory, Oak Ridge, Tennessee 37831, Department of Chemistry and Biochemistry, Eastern Washington University, Cheney, Washington 99004, Clarendon Laboratory, Department of Physics, Oxford University, Oxford, OX1 3PU, U.K., Materials Science Division, Argonne National Laboratory, Argonne Illinois 60439, ISIS Muon Facility, Rutherford Appleton Laboratory, Chilton, Didcot OX11 0QX, U.K., Department of Chemistry, University of Tennessee, Knoxville, Tennessee 37996, Department of Chemistry, Kyung Hee University, Seoul, South Korea 130-701, Department of Chemistry, North Carolina State University, Raleigh, North Carolina 27695-8204

Received August 22, 2006

The mixed-anion coordination polymer $Cu(HCO_2)(NO_3)(pyz)$ was synthesized, its crystal structure was determined by X-ray diffraction, and its magnetic structure was characterized by ac susceptibility, dc magnetization, muon-spin relaxation, and spin dimer analysis. The crystal structure consists of five-coordinate Cu^{2+} ions that are connected through syn–anti bridging μ-HCO_2^- and μ-pyz ligands to form a highly corrugated two-dimensional layered network. Bulk magnetic measurements show a broad maximum in $\chi(T)$ at 6.6 K. The HCO_2^- and pyz ligands mediate ferromagnetic and antiferromagnetic spin exchange interactions between adjacent Cu^{2+} ions with the spin exchange parameters $J/k_B = 8.17$ and -5.4 K, respectively ($H = -J\Sigma S_i \cdot S_j$). The muon-spin relaxation data show a transition to a long-range magnetic ordering below $T_N = 3.66(3)$ K. For $T < T_N$, the $M(H)$ and χ'_{ac} measurements provide evidence for a field-induced spin-flop transition at 15.2 kOe. That $Cu(HCO_2)(NO_3)(pyz)$ undergoes a long-range magnetic ordering is an unexpected result because the one-dimensional $Cu(NO_3)_2(pyz)$ and three-dimensional $Cu(HCO_2)_2(pyz)$ compounds display linear chain antiferromagnetism with no long-range magnetic ordering down to 2 K.

1. Introduction

Ubiquitous oxo-anions such as sulfate (SO_4^{2-}) and nitrate (NO_3^-) are readily found in numerous metal salts and strong acids. Both anions are poor bridging ligands and typically occupy interstitial sites within large frameworks.[1] Acetate ($CH_3CO_2^-$) generally coordinates to two transition metal ions to form dinuclear complexes such as found in $Cu_2(CH_3CO_2)_4 \cdot 2H_2O$ and related compounds.[2] Oxalate ($C_2O_4^{2-}$) has been widely employed as a functional group in the assembly of

* To whom correspondence should be addressed. E-mail: jmanson@ewu.edu. Phone: (509) 359-2878. Fax: (509) 359-6973.
† Oak Ridge National Laboratory.
‡ Eastern Washington University.
§ Oxford University.
£ Argonne National Laboratory.
|| Rutherford Appleton Laboratory.
⊥ University of Tennessee.
Kyung Hee University.
▽ North Carolina State University.

(1) e.g.: (a) Rao, C. N. R.; Sampathkumaran, E. V.; Nagarajan, R.; Paul, G.; Behera, J. N.; Choudhury, A. *Chem. Mater.* **2004**, *16*, 1441. (b) Fan, S. R.; Zhu, L.-G. *Acta. Crystallogr.* **2005**, *E61*, m1689. (c) Yeh, T.-T.; Wu, J.-Y.; Wen, Y.-S.; Liu, Y.-H.; Twu, J.; Tao, Y.-T.; Lu, K.-L. *J. Chem. Soc., Dalton Trans.* **2005**, 656. (d) Carlucci, L.; Ciani, G.; Proserpio, D. *Cryst. Growth Des.* **2005**, *5*, 37. (e) Dronskowski, R.; Liu, X.-H. *Acta. Crystallogr.* **2003**, *C59*, m243. (f) Rujiwatra, A.; Kepert, C. J.; Claridge, J. B.; Rosseinsky, M. J.; Kumagai, H.; Kurmoo, M. *J. Am. Chem. Soc.* **2001**, *123*, 10584. (g) Chen, B.-Q.; Han, L.; Xu, Y.; Wu, B.-L.; Hong, M.-C. *Acta. Crystallogr.* **2004**, *E60*, m1376. (h) Zheng, B,; Liu, G.; Wang, D.-Y.; Hu, H.-M. *Acta. Crystallogr.* **2005**, *E61*, m499. (i) Kutasi, A. M.; Harris, A. R.; Batten, S. R.; Moubaraki, B.; Murray, K. *Cryst. Growth Des.* **2004**, *4*, 605.
(2) (a) Oldham, C. *Prog. Inorg. Chem.* **1968**, *10*, 223. (b) Doedens, R. J. *Prog. Inorg. Chem.* **1976**, *21*, 209.

10.1021/ic061590q CCC: $37.00
Published on Web 12/07/2006

multidimensional magnetic solids such as the two-dimensional (2D) honeycomb array $[(n\text{-Bu})_4\text{N}]\text{Mn}[\text{Fe}(\text{ox})_3]$[3a] and three-dimensional (3D) chiral $[\text{Cr}(2,2'\text{-bipy})_3(\text{BF}_4)[\text{Mn}_2(\text{ox})_3]$.[3b] Surprisingly little attention has been paid to the formate anion HCO_2^- although the malonate anion $(C_3O_4H_2)^{2-}$ has drawn considerable interest.[4] Hydrated transition metal formates such as $Cu(HCO_2)_2(H_2O)_2\cdot 2H_2O$ have long been known and studied even very recently.[5] It has also been possible to replace H_2O in those structures with urea molecules while retaining analogous 2D squarelike grids.[6] Owing to the oxophilic nature of first-row transition metal ions, it seems that Lewis bases such as formate could preferentially combine with those cations to form a rich variety of structure types including mononuclear and polynuclear complexes.

$Cu(NO_3)_2(pyz)$[7] has a uniform one-dimensional (1D) linear chain structure, while $Cu(HCO_2)_2(pyz)$[8] has a 3D framework. The NO_3^- complex is the closest realization to the $S = 1/2$ Heisenberg antiferromagnetic chain ($J/k_B = -10.3$ K) of which the quantum critical state is experimentally accessible.[9] In the formate-derivative, 1D Cu-pyz-Cu chains also exist, but they are further connected via anti−anti bridging HCO_2^- ligands. Magnetically, $Cu(HCO_2)_2(pyz)$ displays a maximum in $\chi(T)$ at 4 K and a fit to a Bonner−Fisher chain model yields $J = -3.94(1)$ K.[8] Bulk magnetic measurements on both $Cu(NO_3)_2(pyz)$ and $Cu(HCO_2)_2(pyz)$ do not show any evidence for long-range order (LRO) down to 1.7 K, while the $C_p(T)$ data on the former down to 0.07 K confirm the 1D nature of the material with no λ-anomaly indicative of LRO being observed.[9] In recent muon-spin relaxation (μ^+-SR) studies on $Cu(NO_3)_2(pyz)$ and $Cu(HCO_2)_2(pyz)$, we identified that the transitions to a long-range magnetic ordering occur below $T_N = 0.107(1)$ and 1.97(8) K, respectively.[10,11] The second moment, Δ, was found to be very similar for the two nitrate-containing materials, which suggests that the muon stopping sites experience similar local nuclear fields.

For the compounds discussed here, the lattice and spin dimensionalities are not necessarily the same.[12] In the case of $Cu(HCO_2)_2(pyz)$, the lattice and spin dimensionalities are three and one, respectively. Although the HCO_2^- anions bridge together the Cu-pyz-Cu chains in $Cu(HCO_2)_2(pyz)$, their contribution to the observed magnetic behavior is largely negligible, as indicated by electronic structure calculations, hence the reason for its reduced spin dimensionality.[8] In the case of $Cu(NO_3)_2(pyz)$, however, the lattice and spin dimensionalities are equivalent and equal to one. In the present work, we describe a markedly different result for the mixed-anion species $Cu(HCO_2)(NO_3)(pyz)$, which can be viewed as a structural and magnetic hybrid between the bis-nitrate and bis-formate complexes. The coordination network of this compound is 2D where single μ-HCO_2^- and pyz units are present and bridge together Cu^{2+} ions. This new hybrid complex magnetically orders below $T_N = 3.66(3)$ K and displays both ferromagnetic and antiferromagnetic interactions.

2. Experimental Section

Synthesis. A 5-mL aqueous solution of $Cu(NO_3)_2\cdot yH_2O$ (3.2 mmol, 0.6000 g) was slowly added to an aqueous solution that contained $NaHCO_2$ (6.7 mmol, 0.4568 g) and pyz (3.2 mmol, 0.2562 g) to afford a deep blue solution. Upon slow evaporation of the solvent at room temperature for 2 weeks, blue needlelike crystals were obtained. The solid was collected via vacuum filtration and air-dried for 6 h giving 0.5195 g of material in 64% yield. Anal. Calcd (%) for $C_5H_5N_3O_5Cu$: C, 23.96; H, 2.01; N, 16.76. Found: C, 23.55; H, 2.00; N, 16.14. Selected IR data (Nujol, cm^{-1}): 3077 w, 3102 w, 1558 s, 1410 s, 1361 s, 1315 s, 1171 m, 1115 m, 1075 m, 1039, 830, and 821 m.

X-ray Crystallography. A small blue rod measuring $0.08 \times 0.08 \times 0.12$ mm^3 was glued to the end of a glass fiber and mounted on a Bruker AXS SMART 1000 X-ray diffractometer equipped with a CCD area detector. The area detector frames were integrated by use of the program SAINT,[13] and the resulting intensities corrected for absorption by Gaussian integration (SHELXTL program suite).[14] The SHELXTL program package was employed in the structure solution using direct methods, full matrix least-squares refinement on F^2 (using all data), and most graphics. All non-hydrogen atoms were refined anisotropically. Formate hydrogen atoms were located by difference Fourier maps but ultimately fixed in calculated positions. Positions of aromatic H atoms were calculated by employing a 'riding' model. No correction for extinction was required. Additional details of the data collection are given in Table 1, while selected bond lengths and angles are listed in Table 2.

Magnetic Measurements. AC susceptibility measurements were conducted on a Lake Shore Cryotronics 7000 series susceptometer equipped with a low-temperature helium subpot option (allowing measurements to as low as 1.5 K to be achieved). A 1-Oe amplitude oscillating at a frequency of 125 Hz was selected for this study. A

(3) (a) Pellaux, R.; Schmalle, H. W.; Huber, R.; Fischer, P.; Hauss, T.; Ouladdiaf, B.; Decurtins, S. *Inorg. Chem.* **1997**, *36*, 2301. (b) Decurtins, S.; Schmalle, H. W.; Pellaux, R.; Schneuwly, P.; Hauser, A. *Inorg. Chem.* **1996**, *35*, 1451.

(4) e.g.: (a) Maji, T. K.; Sain, S.; Mostafa, G.; Lu, T.-H.; Ribas, J.; Monfort, M.; Chaudhuri, N. R. *Inorg. Chem.* **2003**, *42*, 709. (b) Konar, S.; Mukherjee, P. S.; Drew, M. G. B.; Ribas, J.; Chaudhuri, N. R. *Inorg. Chem.* **2003**, *42*, 2545. (c) Ruiz-Perez, C.; Hernandez-Molina, M.; Lorenzo-Ruis, P.; Lloret, F.; Cano, J.; Julve, M. *Inorg. Chem.* **2000**, *39*, 3845. (d) Delgado, F. S.; Sanchiz, J.; Ruiz-Perez, C.; Lloret, F.; Julve, M. *Inorg. Chem.* **2003**, *42*, 5938. (e) Delgado, F. S.; Kerbellac, N.; Ruiz-Perez, C.; Cano, J.; Lloret, F.; Julve, M. *Inorg. Chem.* **2006**, *45*, 1012.

(5) Ronnow, H. M.; McMorrow, D. F.; Harrison, A. *Phys. Rev. Lett.* **1999**, *82*, 3152.

(6) Takeda, K.; Mito, M.; Nakajima, K.; Kakurai, K.; Yamagata, K. *Phys. Rev. B* **2001**, *63*, 024425 and reerences therein.

(7) Santoro, A.; Mighell, A. D.; Reimann, C. W. *Acta. Crystallogr*. **1970**, *B26*, 979.

(8) Manson, J. L.; Lecher, J. G.; Gu, J.; Geiser, U.; Schlueter, J. A.; Henning, R.; Wang, X.; Schultz, A. J.; Koo, H.-J.; Whangbo, M.-H. *J. Chem. Soc., Dalton Trans*. **2003**, *2905*.

(9) Hammer, P. R.; Stone, M. B.; Reich, D. H.; Broholm, C.; Gibson, P. J.; Turnbull, M. M.; Landee, C. P.; Oshikawa, M. *Phys. Rev. B* **1999**, *59*, 1008.

(10) Lancaster, T.; Blundell, S. J.; Brooks, M. L.; Baker, P.; Pratt, F. L.; Manson, J. L.; Landee, C. P.; Baines, C. *Phys. Rev. B* **2006**, *73*, 020410.

(11) Lancaster, T.; Blundell, S. J.; Brooks, M. L.; Baker, P.; Pratt, F. L.; Manson, J. L.; Baines, C. *Phys. Rev. B* **2006**, *73*, 172403.

(12) de Jongh, L. J.; Miedema, A. R. *Adv. Phys.* **1974**, *23*, 1.

(13) Data Integration Software. *SAINT*, version 5.00; Bruker AXS, Inc.: Madison, WI, 1999.

(14) Structure Solution and Refinement Software. *SHELXTL*, version 5.0; Bruker AXS, Inc.: Madison, WI, 1996.

Table 1. X-ray Crystallographic Data for $Cu(HCO_2)(NO_3)(pyz)$

formula	$N_3C_5O_5H_5Cu$
fw, g/mol	250.66
space group	*Pnma*
T, K	173
a, Å	7.700(2)
b, Å	6.777(2)
c, Å	14.851(3)
β, °	90
V, Å^3	775.0(3)
Z	4
ρ_{calc}, g/cm^3	2.148
λ, Å	0.71073
μ, mm^{-1}	2.82
$R(F)^a$	0.0218
$R_w(F)^b$	0.0635
GOF	1.057

^{a} $R = \sum[|F_o| - |F_c|]/\sum|F_o|$. ^{b} $R_w = [\sum w[|F_o| - |F_c|]^2/\sum w[|F_o|^2]]^{1/2}$.

Table 2. Selected Bond Lengths (Å) and Angles (deg) for $Cu(HCO_2)(NO_3)(pyz)$ at 173 K

Cu−O(1)	1.959(2)	C(1)−O(1)	1.265(3)
Cu−O(2A)	1.988(2)	C(1)−O(2)	1.254(3)
Cu−O(3)	2.273(2)	N(1)−C(3)	1.338(2)
Cu−N(1)	2.009(2)	N(2)−O(3)	1.278(3)
Cu−N(1A)	2.009(2)	N(2)−O(4)	1.229(3)
O(1)−Cu−O(2A)	174.07(6)	O(1)−C(1)−O(2)	121.0(2)
O(1)−Cu−N(1)	90.60(4)	O(3)−N(2)−O(4)	119.3(2)
O(1)−Cu−O(3)	81.13(7)	C(2)−N(1)−C(3)	118.1(2)
N(1)−Cu−N(1A)	172.77(8)	Cu−O(2A)−C(1)	105.8(1)
Cu−N(1)−C(2)	123.5(1)	Cu−O(3)−N(2)	128.5(2)

powder sample weighing 114.3 mg was loaded into a Delrin sample holder and affixed to the end of an aluminum rod. The sample was cooled from 300 to 4.5 K over a period of ∼15 min and then further cooled to 1.5 K over a period of ∼45 min. The real and imaginary components, χ' and χ'', respectively, of the volume ac susceptibility were recorded every 0.05 K.

DC magnetization measurements were conducted using Quantum Design MPMS 5.5T SQUID and PPMS 9T magnetometers. Homogeneous powder samples weighing 91.8 (SQUID) or 89.6 mg (PPMS) were loaded into gelatin capsules and mounted on the end of a Quantalloy or carbon fiber rod. The samples were cooled in zero-field to the lowest achievable temperature of 2 K. The magnet was then charged to 1 kOe and data collected on warming up to 300 K. All magnetic data were corrected for core diamagnetism using Pascal's constants.

Muon-Spin Relaxation. Zero-field μ^+SR measurements have been conducted on powder samples using the LTF instrument at the Swiss Muon Source, Paul Scherrer Institut, Villigen, Switzerland and the MuSR instrument at the ISIS facility, Rutherford Appleton Laboratory, UK. Each sample was packed in silver foil and mounted on a silver backing plate. The LTF instrument is based around a dilution refrigerator which has a temperature range of 40 mK to 8 K, while a standard orange cryostat was used on MuSR (base temperature of ∼1.5 K).

In a μ^+SR experiment, spin-polarized positive muons are stopped in a target sample, where the muon usually occupies an interstitial position in the crystal lattice.[15] The observed property in the experiment is the time evolution of the muon spin polarization, the behavior of which depends on the local magnetic field at the muon site. Each muon decays, with a lifetime of 2.2 μs, into two neutrinos and a positron, the latter particle being emitted preferentially along the instantaneous direction of the muon spin. Recording the time dependence of the positron emission directions therefore allows the determination of the spin polarization of the ensemble of muons. In our experiments, positrons were detected by detectors placed forward (F) and backward (B) of the initial muon polarization direction. Histograms $N_F(t)$ and $N_B(t)$ record the number of positrons detected in the two detectors as a function of time following the muon implantation. The quantity of interest is the decay positron asymmetry function, defined as

$$A(t) = \frac{N_F(t) - \alpha N_B(t)}{N_F(t) + \alpha N_B(t)} \quad (1)$$

where α is an experimental calibration constant. $A(t)$ is proportional to the spin polarization of the muon ensemble.

3. Crystal Structure

At 173 K, $Cu(HCO_2)(NO_3)(pyz)$ crystallizes in the orthorhombic space group *Pnma* with $a = 7.700(2)$ Å, $b = 6.777(2)$ Å, $c = 14.851(3)$ Å, and $V = 775.0(3)$ Å^3. The Cu, N(2), O(1), O(2), O(3), O(4), O(5), C(1), and H(1A) atoms reside on the mirror plane (Wyckoff position 4*c*) that lies perpendicular to the *b* axis. Each Cu^{2+} ion has a five-coordinate, distorted square-pyramidal coordination geometry comprised of a CuN_2O_3 chromophore. The axial Cu−O(3) bond length is 2.273(2) Å and is considerably longer than the equatorial Cu−O(1), Cu−O(2), and Cu−N(1) distances, which are 1.959(2), 1.988(2), and 2.009(2) Å, respectively. Bond angles within the CuO_2N_2 basal plane, namely, N(1)−Cu−O(1) and N(1)−Cu−O(2A), are 90.60(4)° and 89.03(4)°, very close to 90°. The N(1)−Cu−N(1A) angle is 172.77(8)°, thus deviating somewhat from linearity. The NO_3^- anion coordinates to the Cu through a single O atom with a Cu−O(3)−N(2) bond angle of 128.5(2)° while two distinctly different Cu−O−C bond angles are observed; Cu−O(1)−C(1) = 133.5(2)° and Cu−O(2)−C(1) = 105.8(1)°. All other bond lengths and angles within the HCO_2, NO_3, and pyz moieties are in good agreement with those typically observed. It should be noted that another mixed formate−nitrate Cu^{2+} complex has been reported, namely, $Cu(HCO_2)(dpyam)(H_2O)(NO_3)$ (dpyam = 2-pyridylamine), which has a 1D zigzag chain structure.[16] However, in this latter compound, the HCO_2^- anion is syn−anti bridging between Cu^{2+} ions while the NO_3^- anion is non-coordinated to the metal center.

A 2D coordination polymer is assembled by bridging μ-HCO_2^- and pyz ligands, as shown in Figure 2 where it can be seen that the formate bridges adopt a *syn-anti* coordinative mode. The Cu−pyz−Cu chains are essentially linear with Cu···Cu separations equal to the *b* axis parameter. The bidentate pyz ligands cross-link Cu−HCO_2−Cu zigzag chains that propagate parallel to the *a* axis with Cu···Cu distances of 4.381 Å leading to a corrugated 2D network. The layers fit together much like a jig-saw puzzle where individual layers are staggered by 1/2*b* to allow the nitrate anions to interdigitate (Figure 3). This leads to close

(15) Blundell, S. J. *Contemp. Phys.* **1999**, *40*, 175.

(16) Youngme, S.; Phuengphai, P.; Chaichit, N.; van Albada, G. A.; Tanase, S.; Reedijk, J. *Inorg. Chim. Acta* **2005**, *358*, 3267.

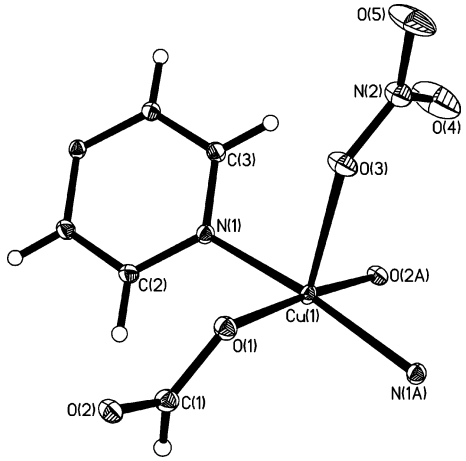

Figure 1. ORTEP drawing and atom labeling scheme for $Cu(HCO_2)(NO_3)(pyz)$. Thermal ellipsoids are drawn at the 35% probability level.

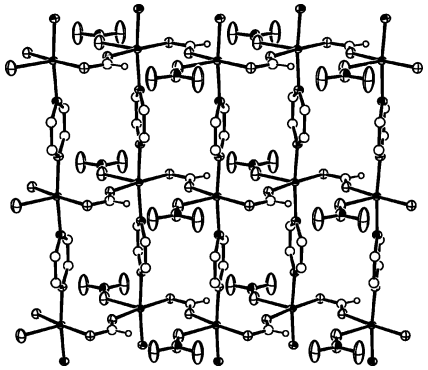

Figure 2. Segment of a single 2D corrugated layer as found in $Cu(HCO_2)(NO_3)(pyz)$. Pyrazine H-atoms have been omitted for clarity.

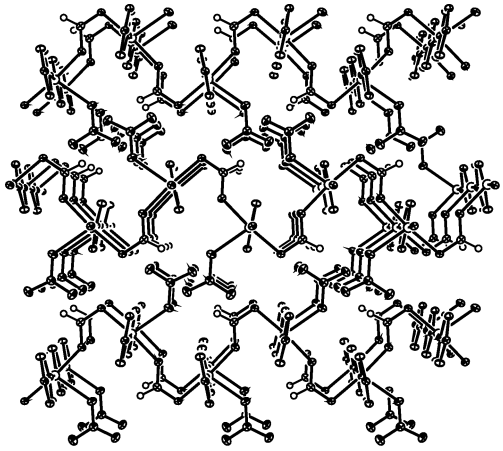

Figure 3. Layer packing diagram for $Cu(HCO_2)(NO_3)(pyz)$ viewed approximately down the *b* axis.

O(2)···H(3A) contacts of 2.523 Å, while the closest interlayer Cu···Cu separation is 6.57 Å.

4. Magnetic Properties

The bulk magnetic properties of $Cu(HCO_2)(NO_3)(pyz)$ were studied by ac susceptibility and dc magnetization techniques. Upon cooling, χ gradually increases, reaching the maximum value of 0.0338 emu/mol at 6.6 K (Figure 4). The broad maximum observed in χ is generally a signature of short-range magnetic ordering (SRO), presumably within

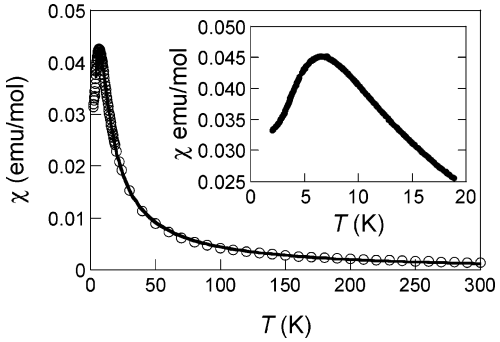

Figure 4. Plot of χ vs T for $Cu(HCO_2)(NO_3)(pyz)$ measured in a 1-kOe magnetic field. The inset highlights the broad maximum observed in the magnetic susceptibility. The solid line in the main figure is a theoretical fit to the data as described in the text.

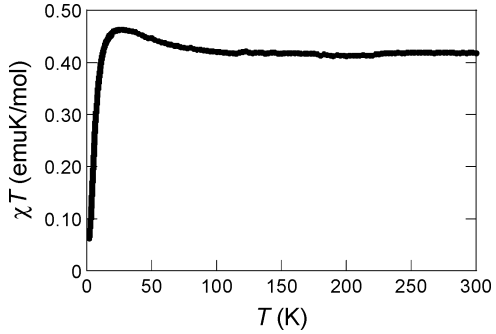

Figure 5. Plot of χT vs T for $Cu(HCO_2)(NO_3)(pyz)$ measured in a 1-kOe magnetic field.

the 2D layers. Upon cooling to 2 K, χ decreases smoothly, reaching a value of 0.025 emu/mol. The decrease in χ may be due to magnetic saturation or increasing antiferromagnetic correlations. A least-squares fit of the $1/\chi$ data to a Curie−Weiss expression ($100 \leq T \leq 300$ K) yields $g = 2.167(3)$ and $\theta = 17.4(6)$ K, suggesting a ferromagnetic contribution to the overall magnetic behavior. At 300 K, the value of χT is 0.394 emuK/mol and only slightly larger than the value of 0.375 emuK/mol expected for isolated $S = 1/2$ Cu^{2+} ions. This behavior is not unusual for this ion, owing to the *g*-tensor anisotropy. Upon cooling from 300 K, χT gradually increases, reaching a broad maximum near 26 K (Figure 5), which indicates the dominance of ferromagnetic interactions between Cu ions. Below this, χT decreases very rapidly due to the build-up of significant antiferromagnetic interactions. From this data alone, there is no clear evidence for a transition to LRO.

The field-dependence of the χ'_{ac} measured at 1.8 K is shown in Figure 6. With increasing H, the susceptibility increases sharply and exhibits a discontinuity at 15.2 kOe and levels off upon increasing the field beyond this value. The isothermal $M(H)$ obtained at 2 K up to 90 kOe shows a gradual upward curvature upon increasing the field, although $M(H)$ does not reach a fully polarized magnetic state (Figure 6). At $H_{dc} = 90$ kOe, the magnetization reaches a value of ~5000 emu·Oe/mol, which is below the expected value of 5585 emu·Oe/mol for $S = 1/2$ (and $g = 2.0$). Assuming a *g*-value of 2.167 as determined from the Curie−Weiss fit of $1/\chi$, the saturation magnetization should be ~6050 emu·Oe/mol. The kink observed in $\chi'(H)$ is likely due to a spin flop transition, which is consistent with the lack of the classic

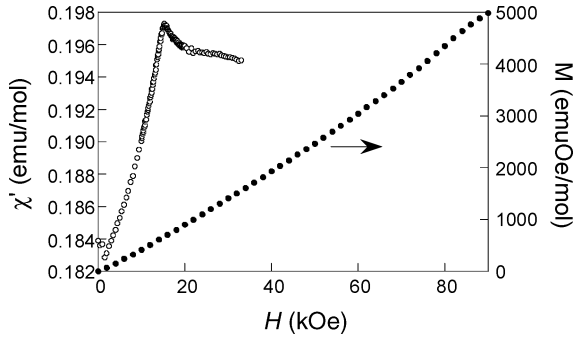

Figure 6. χ'_{ac} (1.8 K, ○) and $M(H)$ (2 K, ●) as a function of dc field for $Cu(HCO_2)(NO_3)(pyz)$.

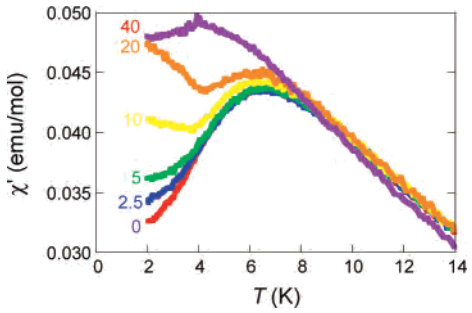

Figure 7. $\chi'(T)$ plots for $Cu(HCO_2)(NO_3)(pyz)$ obtained at $H_{dc} = 0$, 2.5, 5, 10, 20, and 40 kOe.

S-shaped curve in $M(H)$ as expected for a metamagnetic behavior. Furthermore, the upward curving nature of $M(H)$ is typical of low-dimensional quantum-spin magnetic materials.[8,9,17]

Further evidence for a magnetic phase transition is obtained from $\chi'(T)$ data acquired for a variety of applied dc fields (Figure 7). As mentioned above, the data taken for $H_{dc} = 0$ show a smooth decrease upon cooling to 1.5 K. Increasing H_{dc} leads to differing behaviors of χ'. For $H_{dc} =$ 2.5 and 5 kOe, the lower-temperature side of the broad maximum increases with increasing H. At $H_{dc} = 10$ kOe, a clear kink in the data occurs near 4 K, which changes further as H increases to 20 kOe. Finally, at $H_{dc} = 40$ kOe, the broad maximum shifts from 6.6 to 4 K. The dramatic change in the temperature-dependent behavior of χ' between 10 and 20 kOe is consistent with the behavior observed in the $\chi'(H)$ data that show a peak near 15.2 kOe. Suitable single crystals would be required to obtain more information such as the easy-axis direction.

5. Spin Dimer Analysis and Interpretation of the Magnetic Properties

As discussed previously, the adjacent Cu^{2+} ions of $Cu(HCO_2)(NO_3)(pyz)$ are linked by pyz and HCO_2^- bridges. The relative strengths of the spin exchange interactions mediated by these bridges were estimated by performing spin dimer analysis[18] on the basis of extended Hückel tight binding calculations.[19,20] The spin monomer of $Cu(HCO_2)(NO_3)(pyz)$ is given by $[Cu(HCO_2)_2(NO_3)(pyz)_2]^-$. A spin dimer with a pyz unit is given by $[Cu(HCO_2)_4(NO_3)_2(pyz)_3]^{4-}$, and that with HCO_2^- by $[Cu(HCO_2)_3(NO_3)_2(pyz)_4]^{3-}$. These spin dimers each have two singly occupied molecular orbitals (MOs) representing the two spins. The spin orbital interaction energy, Δe, of a spin dimer is obtained as the difference of these two singly occupied MOs. In general, a spin exchange parameter, J, is written as $J = J_F + J_{AF}$. The ferromagnetic term J_F (>0) is small so that the spin exchange becomes ferromagnetic (i.e., $J > 0$) if the antiferromagnetic term J_{AF} (<0) is small in magnitude but becomes antiferromagnetic (i.e., $J < 0$) if the J_{AF} term is large in magnitude. Thus, qualitative trends in spin exchange interactions can be discussed by studying those in their J_{AF} terms. The antiferromagnetic term J_{AF} can be written as

$$J_{AF} \approx -\frac{(\Delta e)^2}{U_{eff}} \qquad (2)$$

where U_{eff} is the effective on-site repulsion. Since U_{eff} is nearly constant for a given system, the trend in the J_{AF} values is explained by studying the associated $(\Delta e)^2$ values. For details of this approach, the readers are referred elsewhere.[18]

Our calculations show that the $(\Delta e)^2$ value for the spin exchange through the pyz bridge is 9000 $(meV)^2$ and nearly zero for the spin exchange through the HCO_2^- bridge. Therefore, it is suggested that the Cu^{2+} ions of $Cu(HCO_2)(NO_3)(pyz)$ form ferromagnetically coupled chains through the HCO_2^- bridges and that these ferromagnetic chains interact antiferromagnetically through the pyz bridges. The resulting 2D spin lattice is a rectangular 2D lattice in which the intrachain spin exchange, J_{intra}, is negative and the interchain spin exchange, J_{inter}, is positive.

In our analysis of the magnetic susceptibility of $Cu(HCO_2)(NO_3)(pyz)$, its 2D spin lattice is treated as pseudo chains, for which the effective susceptibility, χ_{eff}, is expressed in terms of the intrachain susceptibility, χ_{intra}, and the interchain susceptibility, χ_{inter}, as[21]

$$\frac{1}{\chi_{eff}} = \frac{1}{\chi_{inter}} + \frac{1}{\chi_{intra}} \qquad (3)$$

The interchain susceptibility is given by[21,22]

$$\chi_{inter} = -\frac{Ng^2\mu_B^2}{J_{inter}} \qquad (4)$$

(17) e.g.: (a) Landee, C. P.; Turnbull, M. M.; Galeriu, C.; Giantsidis, J.; Woodward, F. M. *Phys. Rev. B* **2001**, *63*, 100402. (b) Woodward, F. M.; Landee, C. P.; Giantsidis, J.; Turnbull, M. M.; Richardson, C. *Inorg. Chim. Acta* **2001**, *324*, 324. (c) Woodward, F. M.; Albrecht, A. S.; Wynn, C. W.; Landee, C. P.; Turnbull, M. M. *Phys. Rev. B* **2002**, *65*, 144412. (d) Willett, R. D.; Galeriu, C.; Landee, C. P.; Turnbull, M. M.; Twamley, B. **2004**, *43*, 3804. (e) Turnbull, M. M.; Albrecht, A. S.; Jameson, G. B.; Landee, C. P. *Mol. Cryst. Liq. Cryst.* **1999**, *335*, 245. (f) Albrecht, A. S.; Landee, C. P.; Slanic, Z.; Turnbull, M. M. *Mol. Cryst. Liq. Cryst.* **1997**, *305*, 333.

(18) For recent reviews, see: (a) Whangbo, M.-H.; Koo, H.-J.; Dai, D. *J. Solid State Chem.* ***2003***, *176*, 417. (b) Whangbo, M.-H.; Dai, D.; Koo, H.-J. *Solid State Sci.* ***2005***, *7*, 827.

(19) Hoffmann, R. *J. Chem. Phys.* **1963**, *39*, 1397.

(20) Our EHTB calculations were carried out by employing the SAMOA program packages (Dai, D.; Ren, J.; Liang, W.; Whangbo, M.-H. http://chvamw.chem.ncsu.edu/.)

(21) Janicki, J.; Troć, R. *J. Phys.: Condens. Matter* **1992**, *4*, 6267.

(22) T. Watanabe, *J. Phys. Soc. Jpn.* **1962**, *17*, 1856.

according to the mean-field approximation, and the intrachain susceptibility is described by the Bonner−Fisher model as[23,24]

$$\chi_{\text{intra}} = \frac{Ng^2\mu_B^2}{k_B T} \frac{0.25 + 0.14995x + 0.30094x^2}{1 + 1.9862x + 0.68854x^2 + 6.0626x^3} \quad (5)$$

where

$$x = \frac{|J_{\text{intra}}|}{k_B T}$$

in the convention where the spin exchange interaction energy between two spin sites is given by the Hamiltonian $H = -J\Sigma S_i \cdot S_j$. The calculated susceptibility to be compared with the experimental data is

$$\chi_{\text{fit}} = \chi_{\text{eff}} + \chi_{\text{TIP}} + \frac{C}{T} \quad (6)$$

where χ_{TIP} refers to the temperature-independent paramagnetism and C is the Curie constant that accounts for a trace amount of paramagnetic impurities. Our least-square fitting analysis leads to the values of $g_{\text{ave}} = 2.14$, $J_{\text{inter}}/k_B = 8.17$ K, $J_{\text{intra}}/k_B = -5.4$ K, $\chi_{\text{TIP}} = -6.84 \times 10^{-5}$ emu/mol and $C = 2.89 \times 10^{-3}$ emu·K/mol, with the standard deviation of 1.64×10^{-4}. As depicted in Figure 4, the experimental susceptibility curve is well described by the calculated curve. Thus, it is reasonable to describe the 2D spin lattice of $Cu(HCO_2)(NO_3)(pyz)$ in terms of a rectangular 2D lattice in which the intrachain spin exchange, J_{intra}, is antiferromagnetic and the interchain spin exchange, J_{inter}, is ferromagnetic. It should be mentioned that J_{intra} is similar to the J-value observed for $Cu(NO_3)_2(pyz)$[9] while J_{inter} is significantly larger than that found ($J = 1.08$ K) for the 1D zigzag chain compound $[Cu(HCO_2)(H_2O)(dpyam)]NO_3$ where dpyam is di-2-pyridylamine.[16]

6. Muon Spin Relaxation

***T* ≤ 3.63 K**. At temperatures below 3.63 K, oscillations in the positron asymmetry are clearly observable. Figure 8a shows an example of a zero-field (ZF) spectrum measured at 0.42 K. These oscillations are characteristic of a quasi-static local magnetic field at the muon site that causes a coherent precession of the spins of those muons with a component of their spin polarization perpendicular to this local field. The frequency of the oscillation is given by $\nu_i = \gamma_m B_i/2\pi$, where γ_m is the muon gyromagnetic ratio ($\equiv 2\pi \times$ 135 MHz/T) and B_i is the local field at the ith muon site. The presence of oscillations in the muon asymmetry for $T \leq 3.6$ K provides strong evidence for the existence of a LRO in this system.

The beating structure of the low-temperature data reflects a contribution from two separate precession frequencies, corresponding to two distinct muon stopping sites in the crystal. The spectra for $T \leq 3.63$ K are found to be most successfully fitted to a function of the form:

$$A(t) = \{A_1 \cos(2\pi\nu_1 t) + A_2 \cos(2\pi\nu_2 t + \phi)\} \exp(-\lambda t) + A_3 \exp(-\Lambda t) + A_{bg} \exp(-\lambda_{bg} t) \quad (7)$$

where λ and Λ are temperature-dependent relaxation rates while A_{bg} and λ_{bg} reflect a temperature-independent contribution to the signal from muons that stop in the silver sample holder or cryostat tail. The term $A_3 \exp(-\lambda t)$ accounts for the contribution from those muons with a spin component parallel to the local magnetic field.

The ratio of the contributions from the oscillating signals A_1/A_2 was found to be ~2:1, which suggests that the site associated with the frequency ν_2 is twice as probable as that associated with ν_1. The origin of the phase offset ϕ ($= -50°$) is unclear, although we note that similar phase offsets have been observed in the μ^+SR studies of $CuCl_2$-(pyz) and $CuBr_2(pyz)$.[25]

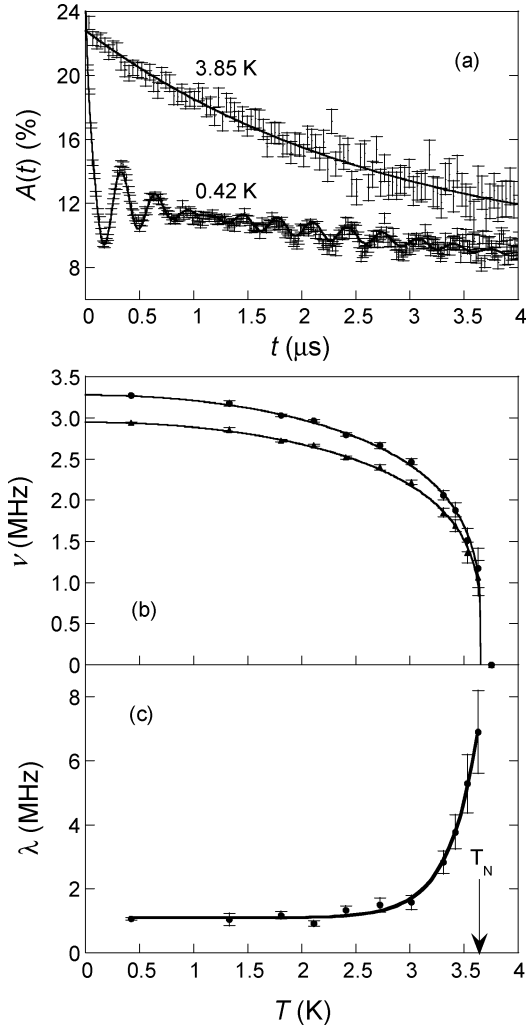

Figure 8. (a) Example asymmetry spectra, $A(t)$, acquired at 0.42 and 3.85 K. (b) Temperature-dependence of the two muon precession frequencies, ν_1 and ν_2. The solid lines represent fits to eq 3 as described in the text. (c) Relaxation rate, λ, as a function of temperature. The solid line serves only as a guide to the eye.

(23) J. C. Bonner and M. E. Fisher, *Phys. Rev.* **1964**, *135*, A640.
(24) J. W. Hall, Ph.D. Dissertation, University of North Carolina at Chapel Hill, 1977. W. E. Hatfield, *J. Appl. Phys.* **1981**, *52*, 1985.
(25) Lancaster, T.; Blundell, S. J.; Pratt, F. L.; Brooks, M. L.; Manson, J. L.; Brechin, E. K.; Cadiou, C.; Low, D.; McInnes, E. J. L.; Winpenny, R. E. P. *J. Phys. Condens. Matter* **2004**, *16*, S4563.

The temperature evolution of the extracted frequencies is shown in Figure 8b. The solid lines represent fits to the expression:

$$\nu_i(T) = \nu_i(0)\left[1 - \left(\frac{T}{T_N}\right)^{\delta}\right]^{\beta} \quad (8)$$

with $\nu_1(0) = 3.28(1)$ MHz (corresponding to a local field at the muon site of $B_1 = 24.2(1)$ mT), $\nu_2(0) = 2.95(1)$ MHz (or $B_2 = 21.8(1)$ mT), $\delta = 2.0(2)$, $\beta = 0.27(3)$, and $T_N = 3.66(3)$ K. Concerning the value of T_N, there is a slight discrepancy between the bulk magnetic susceptibility data, i.e., d(χT)/dT, and the μ^+SR data. We believe the muon results to be more accurate, as muons are a much more sensitive probe to local magnetic fields and spin fluctuations. Importantly, our results highlight the necessity for alternative methods to determine critical temperatures in magnetic compounds. The β exponent determined from the above fit is consistent with a 3D Ising behavior where the theoretical value of 0.312 is expected.[12]

Further evidence for a magnetic phase transition is provided by the temperature dependence of the relaxation rate, λ, which is seen to increase with increasing temperature, diverging as the ordering temperature T_N is approached from below (Figure 8c). This is due to the critical slowing down of magnetic fluctuations in the order parameter, close to the magnetic transition temperature.

***T* ≥ 3.63 K**. An example spectrum measured at temperatures above T_N is shown in Figure 8a. The spectrum shows no significant temperature dependence above the magnetic transition, up to the highest measured temperature (~50 K). Above T_N, the spectra appear Gaussian in form, characteristic of the early time behavior of a Kubo−Toyabe function[26] due to the magnetic field distribution of a static, disordered system, with slow dynamics preventing the characteristic recovery of the polarization at late times. It is likely that the electronic moments are fluctuating too fast compared to the muon time scale and are therefore motionally narrowed from the spectrum. Instead, the muon ensemble is depolarized by the magnetic field distribution at the muon site due to the quasi-static nuclear moments of the surrounding nuclei. This interpretation is supported by the observation that applied fields, B, of magnitude ≥50 G quench the relaxation, as expected for a static distribution.[26]

In order to probe the magnetic field distribution, additional measurements were made at 4.5 and 10 K in applied longitudinal magnetic fields. Example data are shown in Figure 9. The field dependence was found to be identical at 4.5 and 10 K, suggesting that the magnetic phenomenon responsible for the feature observed in the susceptibility near 4.5 K is not effectively probed by the muon. This is not surprising if the muon is indeed only sensitive to the nuclear moments in this regime. For applied fields B_L less than 50 G, the spectra are well described by the longitudinal-field Kubo−Toyabe function,[26] with the addition of a constant term allowing for background contributions as described above. The spectra were therefore fitted to the following function:

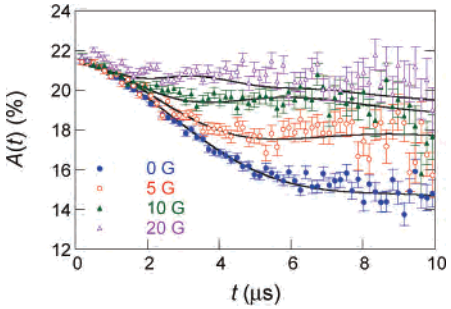

Figure 9. Muon asymmetry spectra acquired at 4.5 K for Cu(HCO$_2$)(NO$_3$)(pyz) obtained in longitudinal fields of 0, 5, 10, and 20 G. Fits shown as solid lines are to the LFKT function as described in the text.

$$A(t) = A_1\left[1 - \left(\frac{2\Delta^2}{\omega_0^2}\right)\left[1 - \exp\left(-\frac{\Delta^2 t^2}{2}\right)\cos\omega_0 t\right] + \left(\frac{2\Delta^4}{\omega_0^3}\right)\int_0^t d\tau \exp\left(-\frac{\Delta^2\tau^2}{2}\right)\sin\omega_0\tau\right] + A_{bg}\exp(-\lambda_{bg}t) \quad (9)$$

Here $\omega_0 = \gamma_m B_L$ and Δ is the second moment of the local magnetic field distribution, fixed at $\Delta = 0.271$ MHz for all values of applied field. For fields ≥50 G, a rise in the initial value of the asymmetry $A(0)$ is observed, characteristic of the repolarization of paramagnetic muon states.[26] The observed increase corresponds to a paramagnetic fraction of ~10% of the total relaxing signal. The observed rise in $A(0)$ was fitted to the standard expression for the repolarization of isotropic muonium,[26] from which we estimate a hyperfine coupling constant, A, of ~200 MHz for these paramagnetic muon states.

We have recently collected μ^+SR data for 1D Cu(NO$_3$)$_2$(pyz) and 3D Cu(HCO$_2$)$_2$(pyz), and while these data have been published elsewhere,[10,11] we will briefly mention the results of these studies as they are relevant to the present discussion. Both Cu(NO$_3$)$_2$(pyz) and Cu(HCO$_2$)$_2$(pyz) have been shown to undergo transitions to a long-range magnetic ordering below $T_N = 0.107(1)$ and 1.97(8) K, respectively, as each shows oscillations in the muon asymmetry function below T_N and a heavily dampened behavior above T_N. The low value of T_N found for Cu(NO$_3$)$_2$(pyz) is to be expected considering that its structure consists of well-isolated 1D linear chains where $J'/J = 4.4 \times 10^{-3}$.[10] In the case of Cu(HCO$_2$)$_2$(pyz), the significantly weaker exchange interactions manifested by the Cu−O−C(H)−O−Cu and Cu−pyz−Cu pathways leads to the reduced Néel temperature.

7. Concluding Remarks

The 2D compound Cu(HCO$_2$)(NO$_3$)(pyz), synthesized and characterized in this work, is a novel structural and magnetic hybrid between 1D Cu(NO$_3$)$_2$(pyz) and 3D Cu(HCO$_2$)$_2$(pyz). This mixed-anion compound shows long-range magnetic ordering below ~3.7 K and a field-induced magnetic phase transition below T_N while the pristine 1D and 3D systems do not show any evidence for a LRO of the magnetic moments down to 2 K. Magnetic measurements combined

(26) Hayano, R. S.; Uemura, Y. J.; Imazato, J.; Nishida, N.; Yamazaki, T.; Kubo, R. *Phys. Rev. B* **1979**, *20*, 850.

with electronic structure calculations have identified two dominant spin exchange pathways, one along the Cu−pyz−Cu chain ($J_{intra}/k_B = -5.4$ K) and the other along the Cu−O−C(H)−O−Cu chain ($J_{inter}/k_B = 8.17$ K). The significantly larger exchange coupling constants and efficient packing of corrugated layers apparently leads to the higher T_N value.

Acknowledgment. Oak Ridge National Laboratory is managed by UT-Battelle, LLC for the U.S. Department of Energy under Contract No. DE-AC05-00OR22725. The work at Argonne National Laboratory is supported by the Office of Basic Energy Sciences, Division of Materials Science, U.S. Department of Energy under Contract No. W-31-109-ENG-38, and that at NCSU under Grant No. DE-FG02-86ER45259. Part of this work was performed at the Swiss Muon Source, Paul Scherrer Institut, Villigen, Switzerland. We are grateful to C. Baines for technical assistance. This work is supported by the EPSRC.

Supporting Information Available: Crystallographic data in CIF format. This material is available free of charge via the Internet at http://pubs.acs.org.

IC061590Q